

Combined methane reforming over nano LaNiO_3 catalyst with modified active surface

Alireza Jahangiri¹ · Majid Saidi^{1,2} · Farhad Salimi³ ·
Abolfazl Mohammadi⁴

Received: 12 August 2017 / Accepted: 4 November 2017
© Springer Science+Business Media B.V., part of Springer Nature 2017

Abstract In this study, nano catalyst LaNiO_3 with perovskite structure was synthesized using the citrate sol–gel method in the combined methane reforming with CO_2 and O_2 (CRM). The effects of increasing the surface area of the LaNiO_3 perovskite on the catalytic activity were investigated by changing the method of preparing and creating holes in the surface of the samples. Physical and chemical properties of the samples, before and after the reactor test, were determined through ICP, AA, XRD, TGA, TPR, BET, SEM, EDX and TEM techniques. The results of XRD, ICP, AA, SEM, EDX and TEM tests indicated that the citrate sol–gel method is a good way to prepare a homogeneous perovskite LaNiO_3 sample on a scale of nanometers. The results of the TPR test showed using etching in the citrate sol–gel method can produce samples with high stability. The BET results indicated that the surface area of the LaNiO_3 sample tripled with the method suggested in this paper. Changes in preparation method lead to induction time decreasing and temperature increasing. Use of etching in the citrate sol gel method had no significant effect in the results of activity tests versus time reaction at a temperature of 800 °C. TGA curves revealed no production of coke over the process for the produced samples.

Keywords Citrate sol–gel method · Nano perovskite catalyst · Substitution · Surface area · CRM process

✉ Alireza Jahangiri
jahangiri@eng.sku.ac.ir

¹ Faculty of Engineering, Shahrekord University, Shahrekord, Iran

² School of Chemistry, College of Science, University of Tehran, PO Box 14155-6455, Tehran, Iran

³ Department of Chemical Engineering, Faculty of Engineering, Kermanshah Branch, Islamic Azad University, Kermanshah, Iran

⁴ Department of Chemical Engineering, University of Bojnord, Bojnord, Iran

Introduction

Today, use of syngas, H_2 and CO , has been recognized as an intermediate for production of clean energy and valuable chemical materials. Production of liquid hydrocarbon fuels with high octane numbers in Fischer–Tropsch process, methanol, aldehydes and alcohols and production of electricity power in fuel cells are all processes that derive from H_2 and CO as the primary materials [1].

The most important process of synthetic gas production is the catalytic reforming process. The primary material of this process is heavy hydrocarbon compounds, natural gas or coal. Since all petroleum resources are reducing, it seems that natural gas is the best choice for the production of syngas. Catalytic processes for converting CH_4 into syngas involve steam (SR), dry (DR) or partial oxidation (POR) reforming of methane [2], individually or in combination. In the DR process, the ratio of H_2 to CO in the product is approximately one, which is appropriate for Fischer–Tropsch reactions. But this process is endothermic and requires high energy [3]. The POR process is exothermic, with the disadvantage of creating hot spots in the catalyst bed, making temperature control difficult. The combined DR and POR processes for syngas production offer the advantages of both processes. In fact, the heat required for the DR reaction is provided by heat released through the PR reaction, and also the possibilities of hot spots and coke aggregation in the catalyst bed are minimized [4, 5]. Recently, use of nano perovskite catalysts (ABO_3) in the methane reforming processes has received special attention due to their significant resistance to coking, high catalytic activity and stability, and the doubly functional role of perovskite catalysts simultaneously as both base and active phases after reduction [6, 7]. In ABO_3 perovskite structures, the A site cation is a lanthanide and/or alkaline earth and the B site cation is a transition metal [8, 9]. Among the preparation methods of perovskite catalysts, the citrate sol–gel method has been acknowledged by researchers as the most efficient and the simplest [10–12]. This method provides the possibility of attaining crystalline particles with nanometer size and high thermal stability. Low active surface area is the greatest weakness of perovskite structures prepared through the sol–gel citrate method. In previous works, we reported the behavior of $La_{1-x}Sm_xNiO_{3-\delta}$ [13], $LaNi_{1-x}Fe_xO_3$ [14], $LaNi_{1-x}Co_xO_3$ [15] and $LaNi_{1-x}Mg_xO_{3-\delta}$ [16] as catalysts in a CRM process in a conventional fixed-bed system. However, all samples showed low surface area as an effective parameter in catalytic evaluations. In this work, the active surface area was increased by making holes in the $LaNiO_3$ perovskite structure. We investigated the catalytic behavior of the $LaNiO_3$ before and after increasing in the surface area through characterization and reactor tests in the CRM Process. For ease in naming, $LaNiO_3$ perovskite catalyst is denoted by the letters A and B in parentheses before and after the change in surface area, respectively.

Experimental

Synthesis of perovskite $LaNiO_3$ (A, B) with citrate sol–gel method

In order to synthesize $LaNiO_3$ (A), first, Citric acid (99% $C_6H_8O_7$, Merck) and ethylene glycol [99% ($C_2H_4(OH)_2$, Merck)] were dissolved in distilled water under

vigorous stirring. Then, nickel nitrate salt [99% (Ni (NO₃)₂·6H₂O, Merck) was added. The molar ratios of citric acid to Ni nitrate and ethylene glycol were 5 and 1, respectively. When Ni nitrate was well dissolved in the solution, stoichiometric quantity of lanthanum nitrate salt [99% La (NO₃)₂·6H₂O, Merck] was added to the solution. The final solution was stirred slowly by magnetic stirrer until the solution was transformed into a gel with high viscosity at an approximate temperature of 60 °C after 12–14 h. The obtained gel was annealed in air at 800 °C for 4 h in an electric furnace for calcination. The heating rate was 1 °C min⁻¹ up to 400 and 3 °C min⁻¹ up to 800 °C [11–13].

Sample LaNiO₃ (B) was prepared in accordance with the method presented by Shu et al. [17]. In this method, zinc nitrate salt [Zn (NO₃)₂·6H₂O, 99%, Merck] was used to create holes on the surface of the LaNiO₃. Thus Zn (NO₃)₂ was introduced into the precursor after the gel formation step. In these experiments, after calcination, Zn (NO₃)₂ was transformed into ZnO and a perovskite structure. Ammonium chloride (NH₄Cl, 99%, Merck) with two molar concentrations under vigorous agitation is required to dissolve ZnO and etch it from the LaNiO₃ perovskite structure. After etching of ZnO for 2 h, the sample was washed twice with deionized water and a vacuum pump and finally re-calcined at 800 °C for 2 h for stabilization of the catalyst structure. During the etching process (Eq. 1), the smell of ammonia indicates the correct procedure of the reaction.



ZnO is used because of its high ionic radius, making hole in the perovskite structure, and also generation of dissoluble ZnO and separation after calcination. The stages producing catalyst LaNiO₃ (A, B) are shown schematically in Fig. 1.

Characterization techniques

Samples were analyzed with different characterization techniques before and after the reactor tests. Perovskite-structure, phase purity and particle size of the catalytic samples were studied before and after the reactor tests using X-ray diffraction (XRD, Phillips PW 1840, $\lambda = 1.54056 \text{ \AA}$). Particle size was determined based on the Scherer equation. Sample morphology was established using scanning electron microscopy (SEM, Philips XL30) and Transmission electron microscopy (TEM, PHILIPS CM200 FEG). Inductively coupled plasma (ICP) emission spectroscopy (Perkin-Elmer ICP/5500) was used to determine the lanthanum and nickel metals. Atomic absorption (AA) spectroscopy (AAS-009 model) was employed for determination of Zn content in the sample. In this study, surface area of the samples was evaluated by a Quantachrom CHEMBET-300 device based on the BET method. To investigate the reduction properties of the samples, the temperature programmed reduction test with TPD/TPR 29000 was done in the range of room temperature up to 850 °C. Quantitative analysis of coke formed on the used catalysts during stability tests were studied using thermal gravity analysis (TG, PL Thermal Science STA 1500).

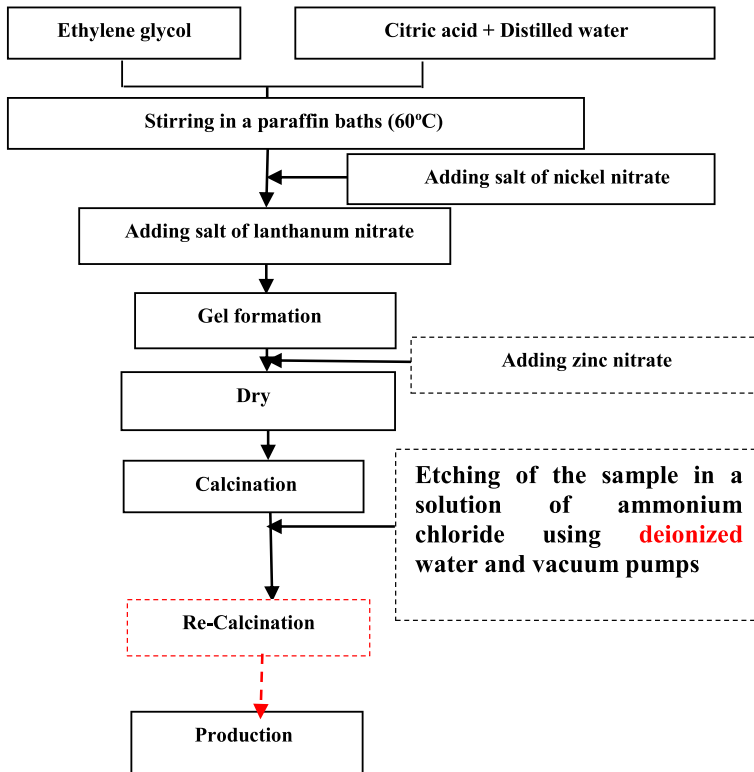


Fig. 1 Steps of LaNiO_3 (A, B) synthesis (steps shown with a dashed line have been added to enhance the active area)

Catalytic activity evaluation

The feed gases (H_2 , CO_2 , CH_4 , O_2 and N_2 , with high-purity of 99%) were entered into a fixed bed quartz reactor with internal diameter of 14 mm and length of 40 cm. The middle part of the reactor was considered as the catalyst loading place, supported by a quartz wool bed. The mass flow controllers (Model 5850, Brooks Instrument, MFC) and monitoring system (Readout, Brooks Instrument) were used after calibration to determine the flow rate of gases entering the reactor. Flow rate of exhaust gas from the reactor was determined using a soap flow meter. A tube furnace was used to heat the reactor. To control the reactor temperature, a temperature indicator (TI) was located in the middle of the catalytic bed. In order to precisely control the catalyst bed, furnace temperature was controlled. For this purpose, another TI was located in the catalyst bed at the furnace chamber and the temperature of the catalytic bed was controlled by controlling the furnace temperature. The temperatures of the furnace and catalyst bed were measured and controlled with two thermocouples (Ni–Cr, K-type, and 0.5 mm diameter) and PID thermo-controllers (Model Jumo iTRON08). A pressure gauge was placed at the top of the reactor in the pathway of the feed gases to indicate the pressure of the system

while performing reactor tests. Operating pressure in this study was one atmosphere. Higher pressure indicates choking in the reactor due to coke formation. The reactants and products were analyzed online by means of a gas chromatograph (Model 6890N, Agilent Technologies), provided with two detectors (FID and TCD) which is capable of determining the amount of reactant and products simultaneously. Star software was used to analyze the data. The schematic of the reactor tests setup is presented in Fig. 2.

Procedure of catalytic activity

In order to investigate the amount of conversion of feed gases (CH₄, CO₂ and O₂) to syngas and the concentration of products, a certain amount of catalyst (0.4 g) was loaded into the reactor. Activity studies for all of the samples were performed under a temperature treatment between 600 and 800 °C and atmospheric pressure. The trend of reactor temperature is shown in Fig. 3.

In order to perform reduction operations, after loading of catalyst, the gas mixture 20% H₂/N₂ was used, with the flow of 50 ml min⁻¹. For this purpose, the reactor bed temperature, with temperature gradient of 5 °C min⁻¹, was increased to 700 °C and maintained for 2 h at 700 °C. Then, the reactor temperature was returned to room temperature under N₂ gas. To evaluate catalytic activity, the CH₄, CO₂, O₂ and N₂ gases were introduced into the reactor with flow rates of 30/30/15/25 ml min⁻¹, respectively. Water produced during the reaction was separated by a silica gel bed. After vapor separation, gas exiting the reactor was entered online into a gas chromatograph (GC). The results were recorded using a computer connected to the GC. In this study, to evaluate the catalytic performance, the CH₄ and CO₂ conversions, $\frac{H_2}{CO}$ and $\frac{H_2}{CH_{4(Conv.)}}$ ratios and H₂ and CO yields are defined as follows [15].

$$CH_4 \text{ conversion (\%)} = \frac{CH_{4,in} - CH_{4,out}}{CH_{4,in}} \times 100$$

$$CO_2 \text{ conversion (\%)} = \frac{CO_{2,in} - CO_{2,out}}{CO_{2,in}} \times 100$$

$$\frac{H_2}{CO} \text{ ratio} = \frac{H_{2,out}}{CO_{out}}$$

$$\frac{H_2}{CH_4(Conv)} \text{ ratio} = \frac{H_{2,out}}{(CH_{4,in} - CH_{4,out})}$$

$$\text{Yield of } H_2 \text{ (\%)} = \frac{\text{moles of } H_2 \text{ produced} \times 100}{2 \text{ moles of } CH_4 \text{ in feed}}$$

$$\text{Yield of } CO \text{ (\%)} = \frac{\text{moles of } CO \text{ produced} \times 100}{\text{moles of } CH_4 \text{ in feed} + \text{moles of } CO_2 \text{ in feed}}$$

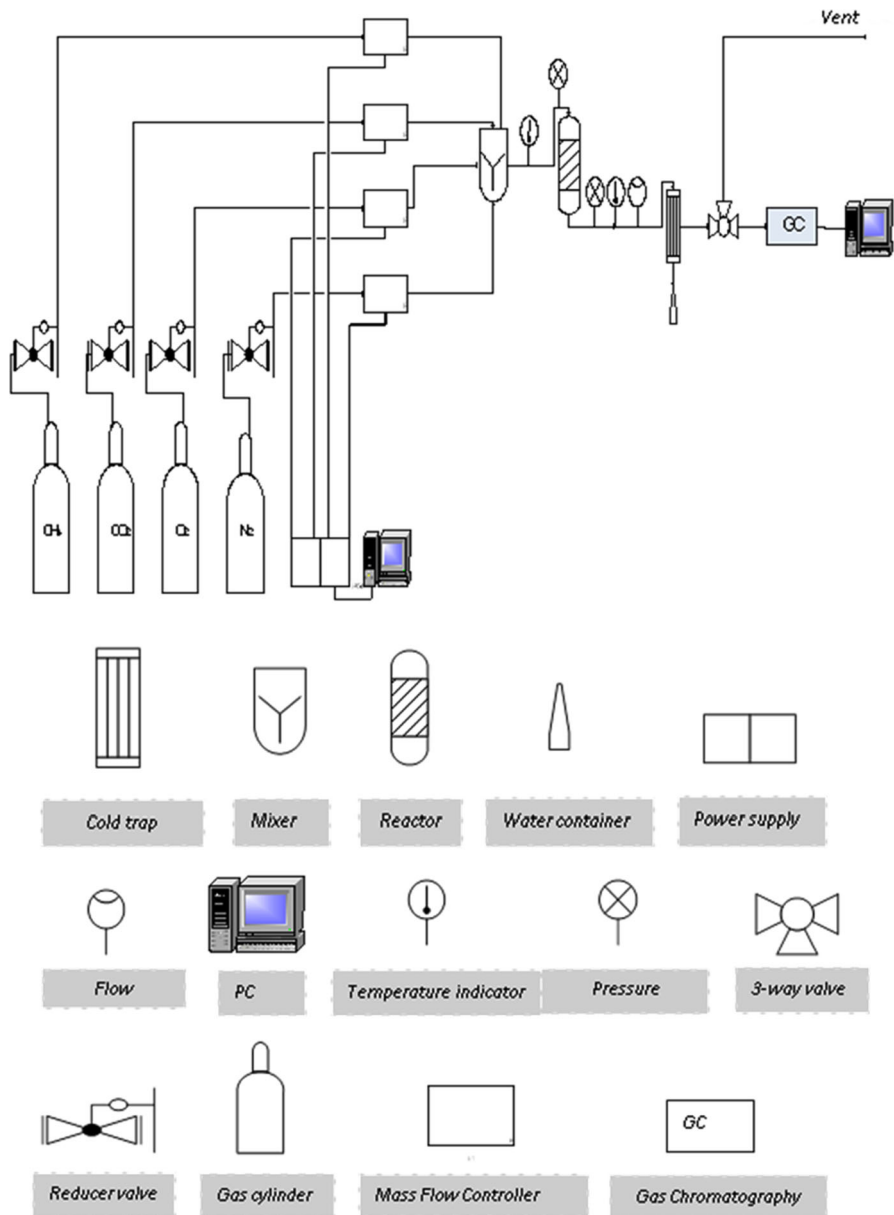


Fig. 2 Schematic of reactor tests system

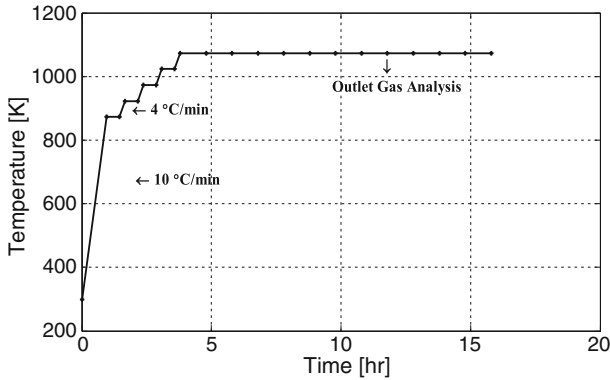


Fig. 3 Thermal treatment used in the CRM process

Results and discussion

Characterization of LaNiO_3 (A, B) samples before the catalytic test

To identify the phases in the samples, X-ray diffraction patterns were measured in the range of 10° – 80° and analyzed using High Score software. The diffraction patterns of LaNiO_3 (A) sample are presented in Fig. 4.

The obtained results showed that the LaNiO_3 (A) sample has a perovskite crystal phase without any other crystalline phases with relatively sharp peaks. The X-ray patterns of this sample were consistent with the referenced X-ray pattern of the sample LaNiO_3 (reference code: 0633-088-01) with rhombohedra phase. These results were in agreement with results presented by others [18, 19]. The LaNiO_3

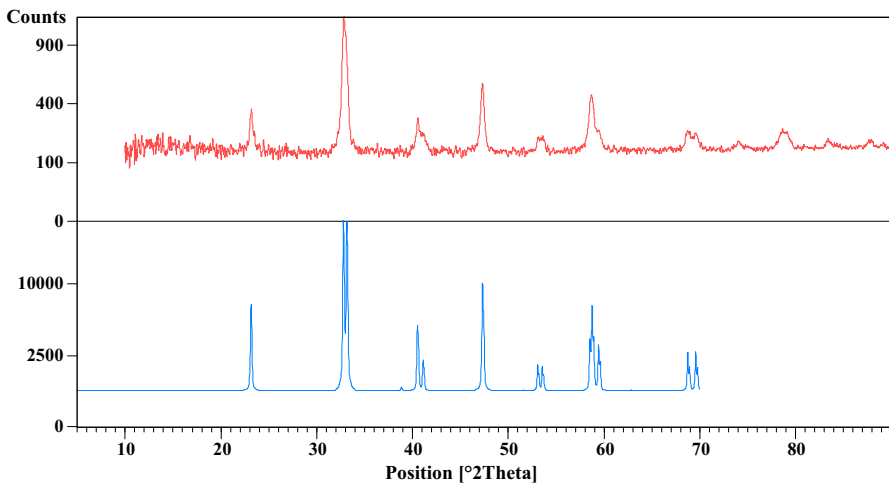


Fig. 4 Real and referenced XRD patterns of LaNiO_3 (A) sample after calcination at 800°C (reference code of LaNiO_3 sample: 0633-088-01)

crystallite size was calculated to be 31 nm at $2\theta = 47.3^\circ$, by applying the Scherer equation. As mentioned in the “[Synthesis of perovskite LaNiO₃ \(A, B\) with citrate sol–gel method](#)” section, in order to increase the active surface area of the LaNiO₃ sample, zinc nitrate and etching operations were used in the final steps of sample preparation. XRD patterns of the LaNiO₃ sample before and after etching are shown in the Fig. 5. As expected, the LaNiO₃ sample before etching has been formed by two phases of LaNiO₃ perovskite and ZnO (reference code: 01-080-0074), although a small amount of NiO with reference code 00-004-0835 is seen as impurity in the sample. After the etching operation, the main phase of the sample was LaNiO₃. However, small amounts of zinc oxide and nickel oxide were detected in XRD patterns. The X-ray diffraction pattern of the LaNiO₃ (B) sample before and after etching with reference patterns are shown in Fig. 5.

Results of BET, ICP and AA tests

The results obtained from the measured weight percentage of metal contents (ICP and AA tests) and surface area (by BET method) of LaNiO₃ perovskite catalyst are presented in Table 1.

The ICP results showed the concentration of Ni and La was close to the nominal values indicating that the citrate sol–gel method is an effective procedure for preparation of the LaNiO₃ (A) sample. However, the etching method led to decreased weight percentage of Ni in the LaNiO₃ (B) sample because of the presence of ZnO compound in the LaNiO₃ (B) structure. The Zn content in the

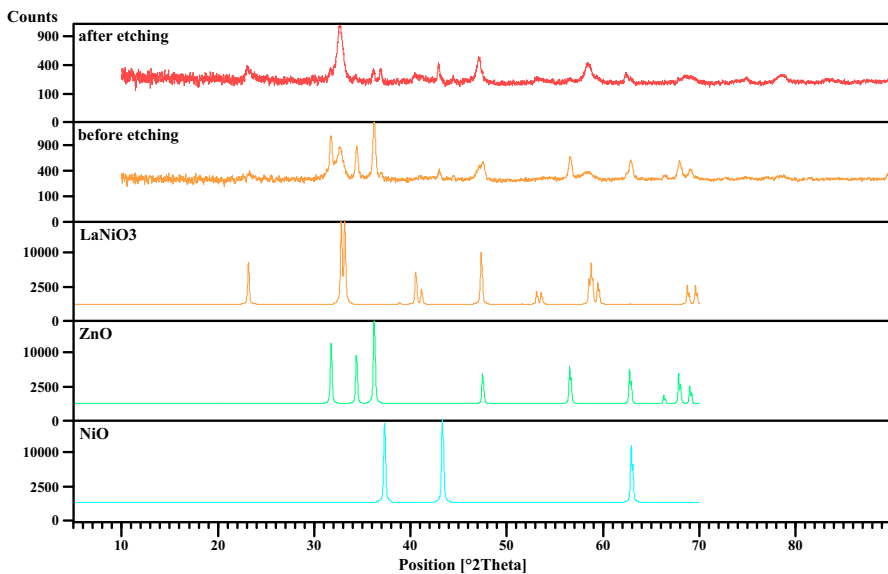


Fig. 5 XRD patterns of LaNiO₃ (B) samples before and after etching process with reference pattern (reference codes of LaNiO₃, ZnO and NiO samples are 0633-088-01, 01-080-0074 and 00-004-0835, respectively)

Table 1 Elemental analysis (by ICP and AA tests), BET surface areas and crystallite size of LaNiO₃ sample before and after etching

	LaNiO ₃ (A)	LaNiO ₃ (B)
La (%)	67.5 (70.3) ^a	68.8 (70.3)
Ni (%)	32.5 (29.7)	26.4 (29.7)
Zn (%)	–	4.5 (0)
surface area (m ² g ⁻¹)	3.15	8.6
Crystal size ^b (nm)	19.6	10.6

^aNominal values of metal contents are presented in parentheses

^bCrystal size of the samples calculated by Scherer equation

sample LaNiO₃ (B) versus weight percent was determined by AA test and is shown in Table 1. The content of Zn was significant and showed that dissolving ZnO and etching it from the LaNiO₃ perovskite structure did not occur correctly, in according with the XRD results.

The specific surface areas of the LaNiO₃ (A) sample were low, which not unexpected, since the LaNiO₃ (A) sample prepared by the citrate sol–gel method and long exposure of the sample with high temperature led to synthesis of low surface area solids. This is consistent with the results reported by other researchers [20]. The LaNiO₃ (B) sample has a surface area of approximately three times more than the LaNiO₃ (A) sample. It seems that presence of Zn with effective ionic radius of 0.75 Å in the etching process could lead to artificial voids in the final structure of LaNiO₃ (B) that increase active surfaces of the sample. This result is in agreement with the findings of Shu et al. [17] on the perovskite structure of LaCoO₃, although they could synthesize this sample with much higher surface area (30 m² g⁻¹).

Results of SEM and TEM tests

In order to estimate the homogeneity of the synthesized solids, LaNiO₃ (A, B) samples were examined by SEM and TEM tests, presented in Fig. 6.

The SEM images showed that LaNiO₃ (A) sample has a uniform nanostructure with approximately spherical particles. According to TEM images of this sample, the particles are in agglomerated and fine form with variable size in the range of 20–40 nm. The particle sizes obtained from the images verified the crystallite sizes that we calculated via the Scherer equation in “[Characterization of LaNiO₃ \(A, B\) samples before the catalytic test](#)” section.

The SEM image of the LaNiO₃ (B) sample was in agreement with XRD results. It seems that big particles in the images were related to ZnO compound as a contaminated phase. The TEM image showed that LaNiO₃ (B) was not spherical in form. However, the particles sizes were in the range of nanometers.

The homogeneity of the system was confirmed by EDX measurements at two points on the samples. The results are presented in Fig. 7.

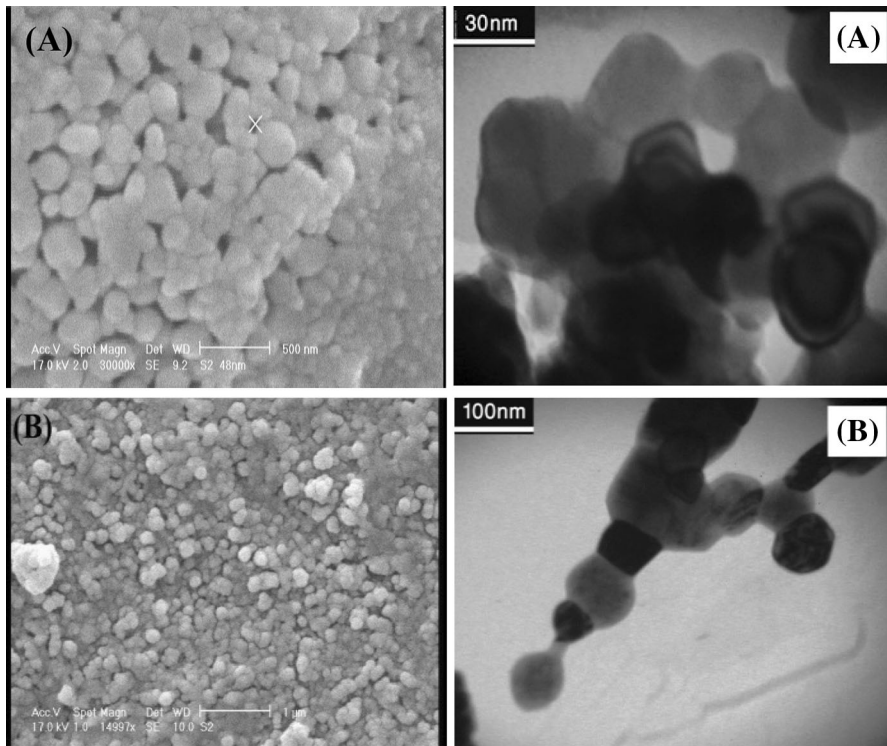


Fig. 6 SEM and TEM images of the calcined LaNiO_3 (A, B) perovskites

Since the preparation method does not include any separation step (crystallization, filtration, etc.) [21], the LaNiO_3 (A, B) samples are in close agreement with those obtained by elemental analysis (“Results of BET, ICP and AA tests” section) and theoretical calculations.

Study on the reducibility of the LaNiO_3 (A, B)

In order to study the reducibility of LaNiO_3 (A, B) samples, TPR experiments were carried out; results are shown in Fig. 8.

The TPR profile of LaNiO_3 (A) showed that this sample is reduced in two main peaks. The first one occurs in the temperature range between 300 and 450 °C, which represents reduction of Ni^{3+} to Ni^{2+} , corresponding to $\text{La}_2\text{Ni}_2\text{O}_5$ formation [22, 23]. The second one occurs at temperatures higher than 450 °C, due to reduction of Ni^{2+} to Ni^0 . The ratio of the second peak to the first peak was 1.9. This ratio should theoretically be equal to 2 [24]. These results were in good agreement with the results of XRD. The following equations show the reduction theory of perovskite LaNiO_3 with H_2 in two stages [25].

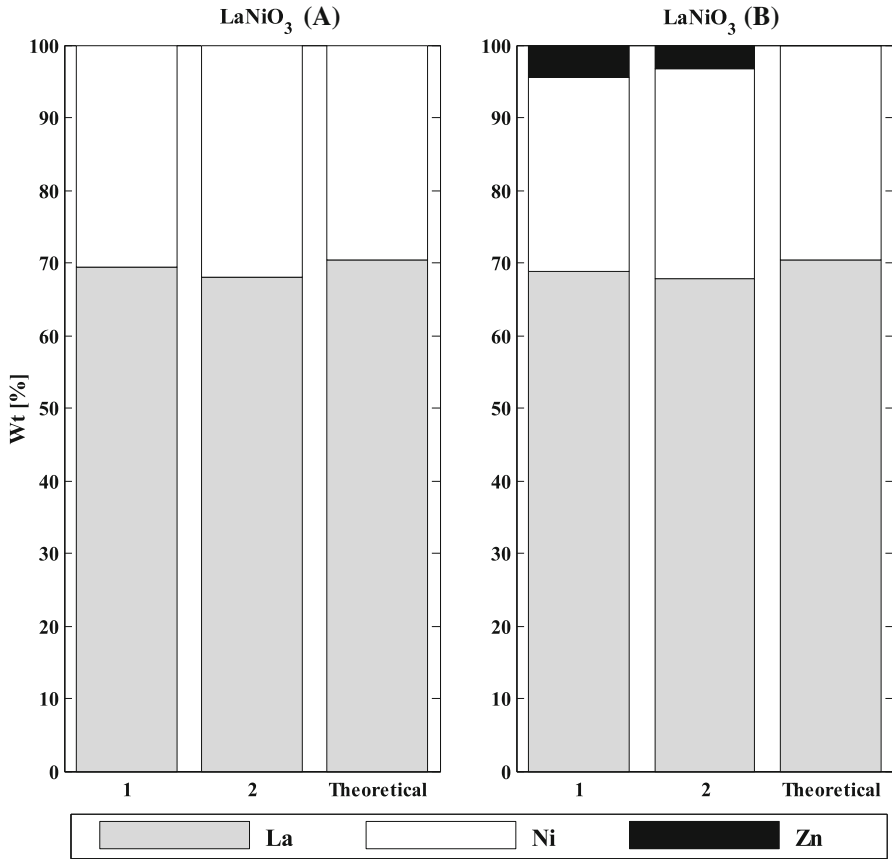


Fig. 7 La, Ni, and Zn distributions observed at two points along the LaNiO_3 (A, B) samples by EDS and the theoretical amounts for calcined at 800 °C

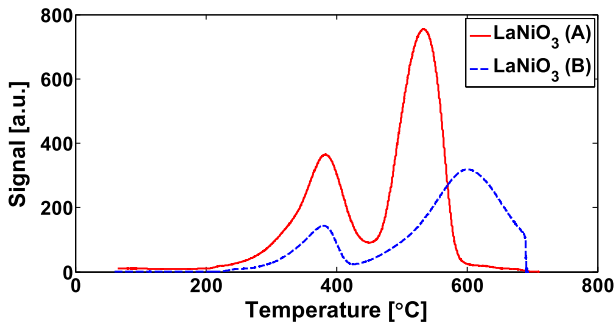
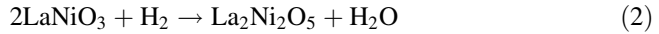


Fig. 8 TPR curves of the calcined LaNiO_3 (A, B) samples



The LaNiO_3 (B) sample is also reduced in two areas. In this case, the first and second reduction peaks occur at higher temperatures. Since the B sample contains ZnO and NiO impurities, the amount of H_2 consumption in the first peak decreases. In this peak, Ni^{3+} decreases into Ni^{2+} . The second peak of reduction was far broader than before. This can be attributed to the presence ZnO and NiO metal oxide and reduction of the Ni^{2+} and Zn^{2+} to Ni^0 and Zn^0 . This confirmed the stabilizing effect of changes in synthesis method on the perovskite structures at higher temperatures.

Activity test

The activity tests of the LaNiO_3 (A, B) samples as a function of reaction temperature were performed in the CRM process. The CH_4 and CO_2 conversions and product yields are shown in Figs. 9 and 10, respectively.

According to Figs. 9 and 10, for both samples, the CH_4 and CO_2 conversions increased with the increase of the reaction temperature. CO_2 conversion was always less than CH_4 . Also, water was produced all of the reaction. It also can be seen that by increasing temperature, the amount of H_2 and CO yields increased and the CO

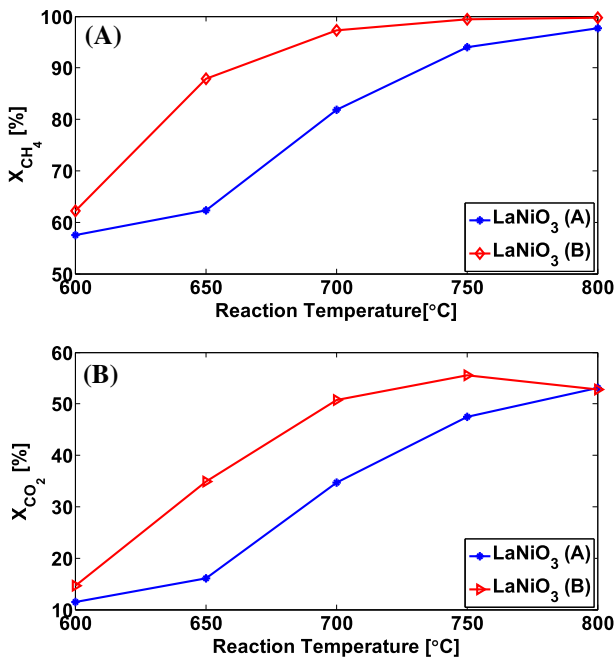


Fig. 9 CH_4 (a) and CO_2 (b) conversion as a function of the reaction temperature for LaNiO_3 (A, B) samples [$\text{CH}_4/\text{CO}_2/\text{O}_2 = 1/1/0.5$, WHSV = 15L/(h g)]

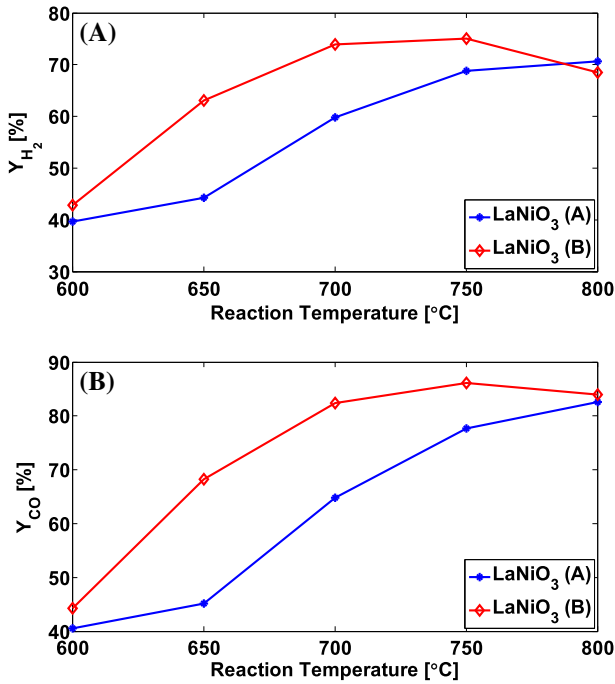
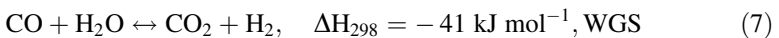


Fig. 10 H₂ (a) and CO (b) yields as a function of the reaction temperature for LaNiO₃ (A, B) [CH₄/CO₂/O₂ = 1/1/0.5, WHSV = 15L/(h g)]

yield was consistently higher than H₂. Tomishige et al. [26] applied Ni/Al₂O₃ and Pt/Al₂O₃ and Rezaie et al. [27] used noble metal catalysts in this process and reported similar results.

These behaviors could be explained by the fact that exothermic CH₄ combustion reactions (Eqs. 4 and 5) at low temperatures and endothermic dry reforming reactions (Eq. 6) and reverse water–gas shift (Eq. 7) at high temperatures were dominant reactions in the CRM process.



On the other hand, CH₄ combustion reactions at low temperatures produced water, CO₂ and CO, which increased the yield of CO in comparison to H₂. From the catalytic perspective, it was observed that induction time (the time required for the precursor perovskite to start showing activity [28]) of the LaNiO₃ (B) sample decreased at temperatures below 800 °C, due higher surface area and stability with

respect to LaNiO_3 (A). In other words, the presence of Zn with high effective ionic radius in this synthesis method could lead to creation of artificial voids in the final structure of LaNiO_3 (B) that increase active surface area and stability of the sample at high temperatures in accordance with BET and TPR results, respectively.

However, when approaching the temperature of 800°C , both samples showed similar catalytic behavior. This showed that the effect of surface area decreased compared to other variables with increasing in reaction temperature.

Catalytic test results of LaNiO_3 (A, B) samples (CH_4 and CO_2 conversions, H_2 and CO yields and $\frac{\text{H}_2}{\text{CO}}$ and $\frac{\text{H}_2}{\text{CH}_4(\text{Conv.})}$ ratios) in terms of reaction time in temperature of 800°C in the CRM process are presented in Figs. 11, 12 and 13.

As illustrated in these figures, LaNiO_3 (A,B) samples show a similar behavior at a temperature of 800°C , and even the sample with lower active surface area, [LaNiO_3 (A)], shows better catalytic behavior, due to uniform distribution of active phase (Ni^0) in the crystal lattice of perovskite. According to the results of XRD, ICP and AA tests, the Zn element in a small amount was substituted by Ni in the perovskite structure of the LaNiO_3 (B) sample and reduced the uniformity of the sample (B), as seen in the SEM and TEM images.

In fact, from the catalytic point of view, a contrast existed between the crystalline structure and surface area and stability in this study. Since change in the surface area and stability of the LaNiO_3 were low due to modifications in preparation of the

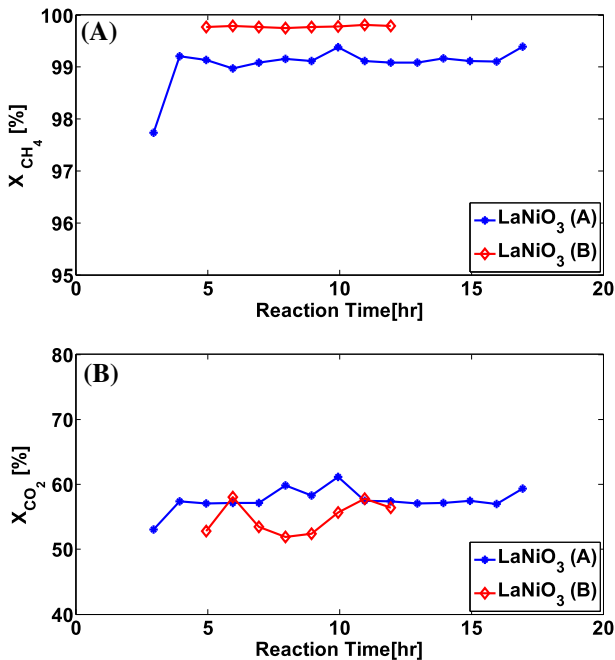


Fig. 11 CH_4 (a) and CO_2 (b) conversion as a function of the reaction time for LaNiO_3 (A, B) [$\text{CH}_4/\text{CO}_2/\text{O}_2 = 1/1/0.5$, $\text{WHSV} = 15\text{L}/(\text{h g})$]

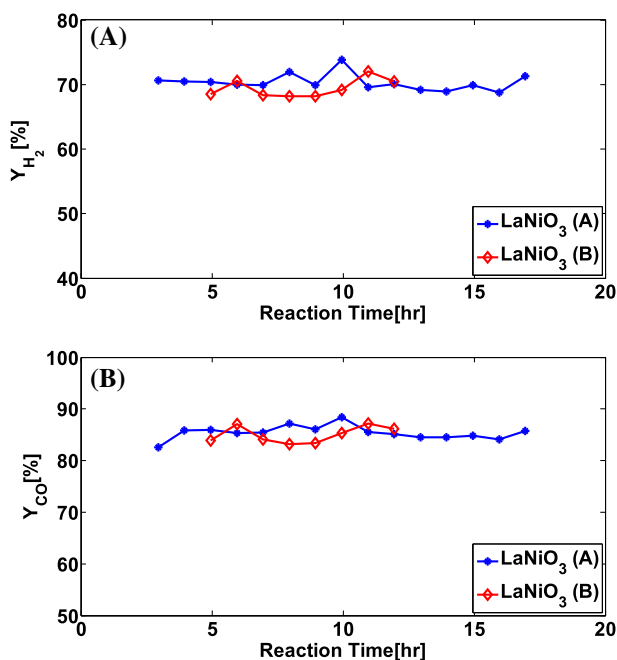
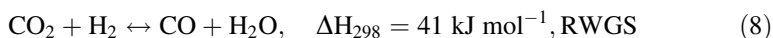


Fig. 12 H₂ (a) and CO (b) yields as a function of the reaction time for LaNiO₃ (A, B) [CH₄/CO₂/O₂ = 1/1/0.5 WHSV = 15 L/(h g)]

catalyst, thus these variables had fewer effects compared to the distribution crystal structure at 800 °C.

Regarding the feed ratio, the ratios of $\frac{H_2}{CO}$ and $\frac{H_2}{CH_{4(Con\text{v.})}}$ were, respectively, less and more than one. This shows that reactions (6) and (8) were carried out as the main reactions in the temperature of 800 °C.



Physical and chemical characterization of the samples after the activity test

XRD tests and the Scherer equation were used in order to study the crystal structure of LaNiO₃ (A, B) samples and determine the crystal size of nickel. The obtained results are shown in Fig. 14 and Table 2.

The crystal structure of LaNiO₃ (A, B) samples, after the reactor test, were completely different from those of the fresh samples. Crystal structure of LaNiO₃ was lost to form of the La₂O₂CO₃ (reference code No: 01-084-1963), La(OH)₃ (reference code No: 01-075-1900) and Ni⁰ (reference code No: 01-087-0712) phases. The La₂O₂CO₃ structure, in accordance with the following equation (Eq. 9), plays an important role in the removal of coke produced during the CRM process [25].

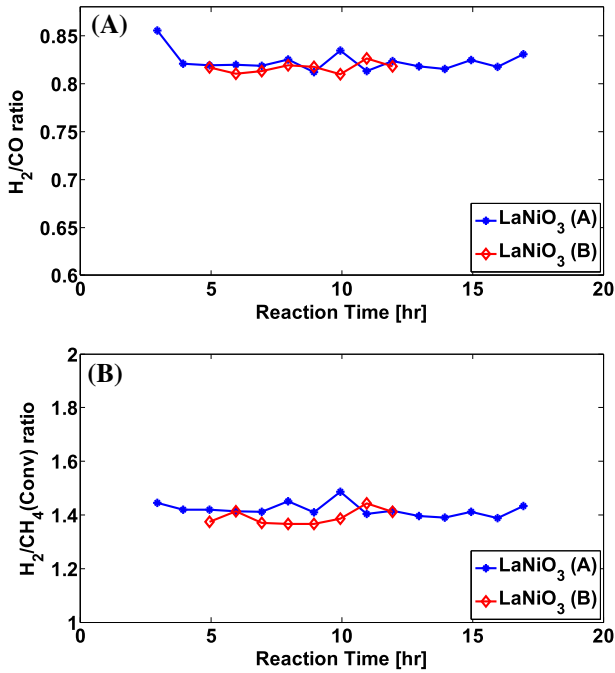
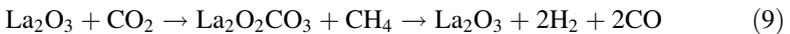
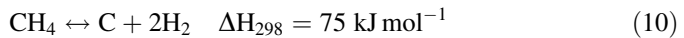


Fig. 13 $\frac{H_2}{CO}$ (a) and $\frac{H_2}{CH_4(Conv)}$ (b) ratios as a function of the reaction time for LaNiO₃ (A, B) [CH₄/CO₂/O₂ = 1/1/0.5, WHSV = 15L/(h g)]



As mentioned, from the catalytic point of view, the main factors for conversion of CH₄ and CO₂ gases in the reaction were in the structure of LaNiO₃, Ni⁰ and La₂O₃ phases, after reduction and during the CRM process. On the other hand, the main factor of coke production at high temperatures in CRM process was endothermic reaction of CH₄ decomposition (Eq. 10). Therefore, according to Eq. 9, presence of La₂O₂CO₃ in the catalyst structure not only reflects ease of CH₄ conversion, but also prevents coke formation and reproduces La₂O₃ compound to the reaction of CO₂ with it. La(OH)₃ phases have been produced due to hydrolysis of La₂O₃ with water during the reaction and exposure of the used catalyst with atmospheric moisture. The presence of the metallic active phase (Ni⁰) was a reason for appropriate catalytic behavior in all samples.



On the other hand, presence of O₂ in the feed of CRM, according to Eq. 11, resulted in burning of coke produced during the process, such that no peaks were observed related to coke in the XRD results.

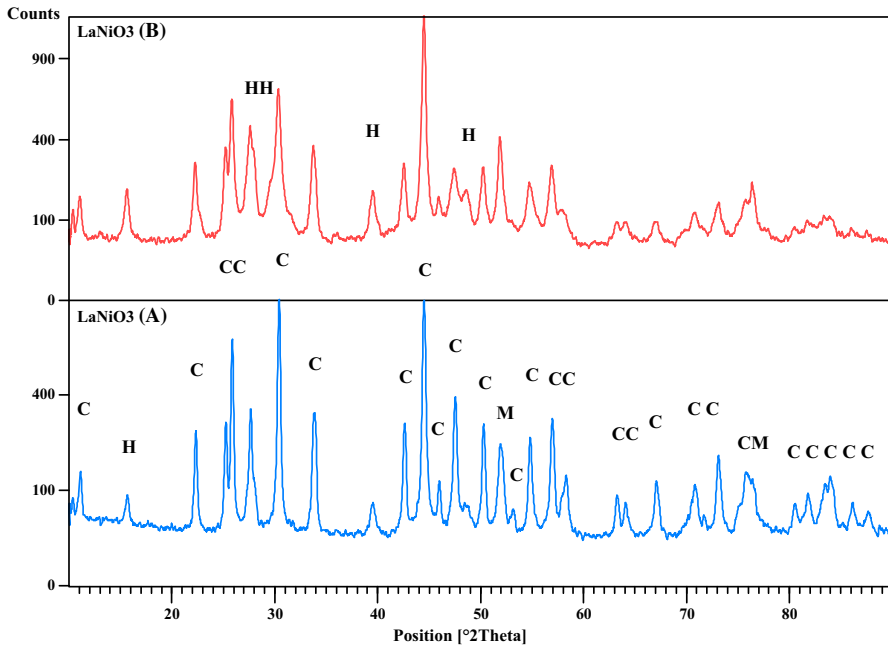
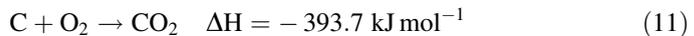


Fig. 14 XRD patterns of LaNiO₃ (A, B) samples after CRM process [CH₄/CO₂/O₂ = 1/1/0.5, WHSV = 15L/(h g), reaction temperature = 800 °C] La₂O₂CO₃ (C), La (OH)₃ (H), Ni⁰ (M)

Table 2 Results of nickel particle size and coke formation rate for LaNiO₃ (A, B) after CRM process

Catalyst	Rate of coke formation	Size of nickel particle (nm)	Reaction time (h)
LaNiO ₃ (A)	0.005	24	16.95
LaNiO ₃ (B)	0.009	22	11.95

The unit of coke formation rate: [mol of carbon mol⁻¹ of (CH₄ + CO₂)_{converted} h⁻¹]



The crystal structure of LaNiO₃ (B) was very similar to the LaNiO₃ (A) sample after the activity test, with a difference in the peaks of the La(OH)₃ phase, which were sharper than the peaks in sample (A). The lower percentage of CO₂ conversion in this sample can be attributed to the presence of La (OH)₃, among others. By comparing the sizes of nickel metallic crystals in these two samples, it was found that both structures have the same size, although it seems that nickel has been less agglomerated in the LaNiO₃ (B) sample in comparison with XRD results of the “[Characterization of LaNiO₃ \(A, B\) samples before the catalytic test](#)” section.

The TGA test was used to study the coke produced in the CRM process (Fig. 15). The coke-calculated theoretical values are presented in the Table 2. For LaNiO₃ (A, B) samples, TGA curves approximately did not represent coke formation.

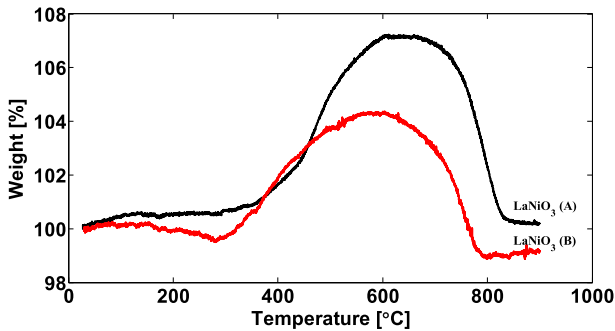


Fig. 15 TGA curves of the LaNiO_3 (A, B) catalysts after the stability test (feed ratio $\text{CH}_4/\text{CO}_2/\text{O}_2 = 1/1/0.5$, reaction temperature = 800 °C)

These results confirmed the results obtained from the coke theory amounts. According to the TGA curves, it was not possible to study in detail the relationship between method of preparation and the amount of coke deposition because of the very small amount of coke produced. However, due to the oxidation of the metallic active sites (weight increase) overlapping with oxidation of carbon deposits (weight loss), the quantification of the deposited carbon was not always accurate. The results of TGA were consistent with XRD analysis after the activity test.

Conclusions

The results of characterization and reactor tests of the catalysts in this study can be summarized as follows:

1. ICP and AA tests and EDX results showed that nickel percentage decreased in the structure of the LaNiO_3 sample when an etching method was used in preparation.
2. Results of XRD patterns indicated that both LaNiO_3 (A, B) samples had approximately the same crystalline structure after calcinations.
3. The BET test results showed surface area of LaNiO_3 sample tripled after etching.
4. SEM and TEM images revealed that the LaNiO_3 (A) sample has an approximately spherical uniform nanostructure. The particles were in compact shape with variable size in the range of 20–40 nm. SEM images of the LaNiO_3 (B) sample showed the perovskite structure also has a contaminating phase. The TEM image of this sample also showed that the shape of the particles, despite the nanostructure, was not necessarily spherical.
5. According to the TPR analysis results, two LaNiO_3 (A, B) perovskite samples were reduced in two areas. The first and second reduction stages for the LaNiO_3 (B) sample occurred at higher temperatures and made the metal reduction more difficult.
6. Changes in preparation method to enhance the surface area led to induction time decreasing with temperature increasing. However, use of etching in the citrate

sol-gel method had no significant effect on results of activity tests versus time reaction at a temperature of 800 °C.

Acknowledgements The authors gratefully acknowledge the financial support of this work by Iranian National Science Foundation. Funding was provided by Iran National Science Foundation (Grant No. 93038553).

References

1. S.K. Chawl, M. George, F. Patel, S. Patel, *Proc. Eng.* **51**, 461–466 (2013)
2. H. Eltejaei, H. Reza Bozorgzadeh, J. Towfighi, M. Reza Omidkhah, M. Rezaei, R. Zanganeh, A. Zamaniyan, A. Zarrin Ghalam, *Int. J. Hydrogen Energy* **37**, 5 (2012)
3. A. Moniri, S.M. Alavi, M. Rezaei, *J. Nat. Gas Chem.* **19**, 6 (2010)
4. M. Zangouei, A. Zarringhalam Moghaddam, A. Razeghi, R. Omidkhah Mohammad, *Int. J. Chem. Reactor Eng.* **8**, 1 (2010)
5. M.R. Goldwasser, M.E. Rivas, M.L. Lugo, E. Pietri, J. Pérez-Zurita, M.L. Cubeiro, A. Griboval-Constant, G. Leclercq, *Catal. Today* **107–108**, 106–113 (2005)
6. M.S.S. Khine, L. Chen, S. Zhang, J. Lin, S.P. Jiang, *Int. J. Hydrogen Energy* **38**, 30 (2013)
7. G. Valderrama, C. Urbina de Navarro, M.R. Goldwasser, *J. Power Sources* **234**, 31–37 (2013)
8. G.R. Moradi, M. Rahmanzadeh, F. Khosravian, *J. CO₂ Util.* **6**, 7–11 (2014)
9. Z. Wang, C. Wang, S. Chen, Y. Liu, *Int. J. Hydrogen Energy* **39**, 11 (2014)
10. S.M. Sajjadi, M. Haghighi, F. Rahmani, *J. Sol-Gel. Sci. Technol.* **70**, 1 (2014)
11. L. Predoana, B. Malic, M. Kosec, M. Carata, M. Caldaru, M. Zaharescu, *J. Eur. Ceram. Soc.* **27**, 13–15 (2007)
12. M.R. Goldwasser, M.E. Rivas, E. Pietri, M.J. Pérez-Zurita, M.L. Cubeiro, A. Griboval-Constant, G. Leclercq, *J. Mol. Catal. A: Chem.* **228**, 1–2 (2005)
13. A. Jahangiri, H. Pahlavanzadeh, H. Aghabozorg, *Int. J. Hydrogen Energy* **37**, 13 (2012)
14. A. Jahangiri, H. Aghabozorg, H. Pahlavanzadeh, *Int. J. Hydrogen Energy* **38**, 25 (2013)
15. A. Jahangiri, H. Aghabozorg, H. Pahlavanzadeh, J. Towfighi, *Int. J. Chem. Reactor Eng.* **12**, 25 (2014)
16. A. Jahangiri, M. Saidi, A. Mohammadi, M. Sedighi, *Int. J. Chem. React. Eng.* **59**, 1–15 (2017). <https://doi.org/10.1515/ijcre-2017-0059>
17. J. Shu, S. Kaliaguine, *Appl. Catal. B* **16**, 4 (1998)
18. R. Pereñíguez, V.M. González-DelaCruz, J.P. Holgado, A. Caballero, *Appl. Catal. B* **93**, 3–4 (2010)
19. G.R. Moradi, M. Rahmanzadeh, *Catal. Commun.* **26**, 169–172 (2012)
20. M.R. Goldwasser, V.E. Dorantes, M.J. Pérez-Zurita, P.R. Sojo, M.L. Cubeiro, E. Pietri, F. González-Jiménez, Y.N. Lee, D. Moronta, *J. Mol. Catal. A: Chem.* **193**, 227–236 (2003)
21. L. Bedel, A.C. Roger, C. Estournes, A. Kiennemann, *Catal. Today* **85**, 2 (2003)
22. M.T. Anderson, J.T. Vaughey, K.R. Poeppelmeier, *Chem. Mater.* **5**, 2 (1993)
23. J.L.G.F.M.E. Rivas, M.R. Goldwasser, E. Pietri, M.J. Pérez-Zurita, G.L.A. Griboval-Constant, *Appl. Catal. A* **344**, 10–19 (2008)
24. H. Arandiyán, J. Li, L. Ma, S.M. Hashemnejad, M.Z. Mirzaei, J. Chen, H. Chang, C. Liu, C. Wang, L. Chen, *J. Ind. Eng. Chem.* **18**, 6 (2012)
25. G. Valderrama, A. Kiennemann, M.R. Goldwasser, *Catal. Today* **133–135**, 142–148 (2008)
26. K. Tomishige, S. Kanazawa, M. Sato, K. Ikushima, K. Kunimori, *Catal. Lett.* **84**, 1 (2002)
27. B. Nematollahi, M. Rezaei, M. Khajenoori, *Int. J. Hydrogen Energy* **36**, 4 (2011)
28. M.R. Goldwasser, M.E. Rivas, E. Pietri, M.J. Pérez-Zurita, M.L. Cubeiro, L. Gingembre, G. Leclercq, *Appl. Catal. A* **255**, 45–57 (2003)